AGU ADVANCING EARTH AND SPACE SCIENCES

Geophysical Research Letters®

RESEARCH LETTER
10.1029/2023GL103673

Constraints on the Cryohydrological Warming of Firn and Ice in Greenland From Rayleigh Wave Ellipticity Data

G. A. Jones[1,2], A. M. G. Ferreira[2,3], B. Kulessa[1,4], M. Schimmel[5], A. Berbellini[6], and A. Morelli[6]

[1]School of Bioscience, Geography and Physics, Swansea University, Swansea, UK, [2]Department of Earth Sciences, University College London, London, UK, [3]CERIS, Instituto Superior Técnico, Universidade de Lisboa, Lisboa, Portugal, [4]University of Tasmania, Hobart, TAS, Australia, [5]Geosciences Barcelona (GEO3BCN-CSIC), Barcelona, Spain, [6]Istituto Nazionale di Geofisica e Vulcanologia, Bologna, Italy

Abstract Rayleigh wave ellipticity measurements from seismic ambient noise recorded on the Greenland Ice Sheet (GrIS) show complex and anomalous behavior at wave periods sensitive to ice ($T < 3$–4 s). To understand these complex observations, we compare them with synthetic ellipticity measurements obtained from synthetic ambient noise computed for various seismic velocity and attenuation models, including surface wave overtone effects. We find that in dry snow conditions within the interior of the GrIS, to first order the anomalous ellipticity observations can be explained by ice models associated with the accumulation and densification of snow into firn. We also show that the distribution of ellipticity measurements is strongly sensitive to seismic attenuation and the thermal structure of the ice. Our results suggest that Rayleigh wave ellipticity is well suited for monitoring changes in firn properties and thermal composition of the Greenland and Antarctic ice sheets in a changing climate.

Plain Language Summary Surface meltwater is increasingly being routed and distributed through the Greenland Ice Sheet (GrIS) changing the mechanical and thermal properties of the ice and resulting in accelerated ice flow. Here we observe complex and anomalous Rayleigh wave ellipticity measurements at periods sensitive to the ice structure. We compare our observations with ellipticity measurements made on simulated seismic noise for various seismic velocity and attenuation models. We demonstrate that in the interior of the GrIS the ellipticity is sensitive to the accumulation and densification of snow as it compacts into glacier ice. The variation in the measurements is strongly sensitive to the thermal structure of the ice sheet which we estimate to be warmer than about −10°. These results demonstrate that Rayleigh wave ellipticity is well suited for monitoring changes in firn properties and thermal composition of the Greenland and Antarctic ice sheets in a changing climate.

Key Points:

- Densification of snow into firn has a first order effect on ellipticity measurements at periods sensitive to the ice
- The distribution of ellipticity measurements is sensitive to the thermal composition of the ice
- Ellipticity is a promising method for long term monitoring of ice properties and thickness beneath the seismic station

Supporting Information:

Supporting Information may be found in the online version of this article.

Correspondence to:

G. A. Jones,
glennarthurjones@gmail.com

Citation:

Jones, G. A., Ferreira, A. M. G., Kulessa, B., Schimmel, M., Berbellini, A., & Morelli, A. (2023). Constraints on the cryohydrological warming of firn and ice in Greenland from Rayleigh wave ellipticity data. *Geophysical Research Letters*, *50*, e2023GL103673. https://doi.org/10.1029/2023GL103673

Received 21 MAR 2023
Accepted 22 JUN 2023

1. Introduction

The Greenland Ice Sheet (GrIS) is experiencing accelerating ice mass loss, accounting for ∼10% of mean global sea level rise since 1990 (Abram et al., 2019; Change, 2014). Surface melt during the summer is now two to five times greater than pre-industrial levels (Abram et al., 2019) and is increasingly being routed and distributed throughout the GrIS, changing both the mechanical and thermal properties of the ice-column. Over time this leads to cryohydrological warming of the ice and faster ice flow (e.g., Cuffey & Paterson, 2010; Phillips et al., 2010). In addition, amplified routing of meltwater to the base of the GrIS will enlarge and expand basal networks of efficient drainage channels, slowing the ice flow speed (e.g., Davison et al., 2019). Hydrological forcing will therefore result in a complex response of the ice sheet to climate warming.

Traditionally, reflection surveys have been the primary seismic approach used to constrain ice properties (e.g., Anandakrishnan et al., 1998; Booth et al., 2012; Peters et al., 2012). However, developments in seismic ambient noise methods offer a relatively cheap alternative to such surveys. In Greenland to date, ice-related studies based on seismic noise interferometry have primarily been used to infer relative changes in the subglacial environment (Mordret et al., 2016; Toyokuni et al., 2018). However, due to large inter-station distances on the GrIS these approaches are not ideally suited to study the ice structure. Alternatively, measurements of Rayleigh wave ellipticity, the horizontal-to-vertical (H/V) ratio of Rayleigh wave particle motion, are sensitive to the subsurface structure directly below the measurement station (e.g., Ferreira & Woodhouse, 2007). Ellipticity measurements

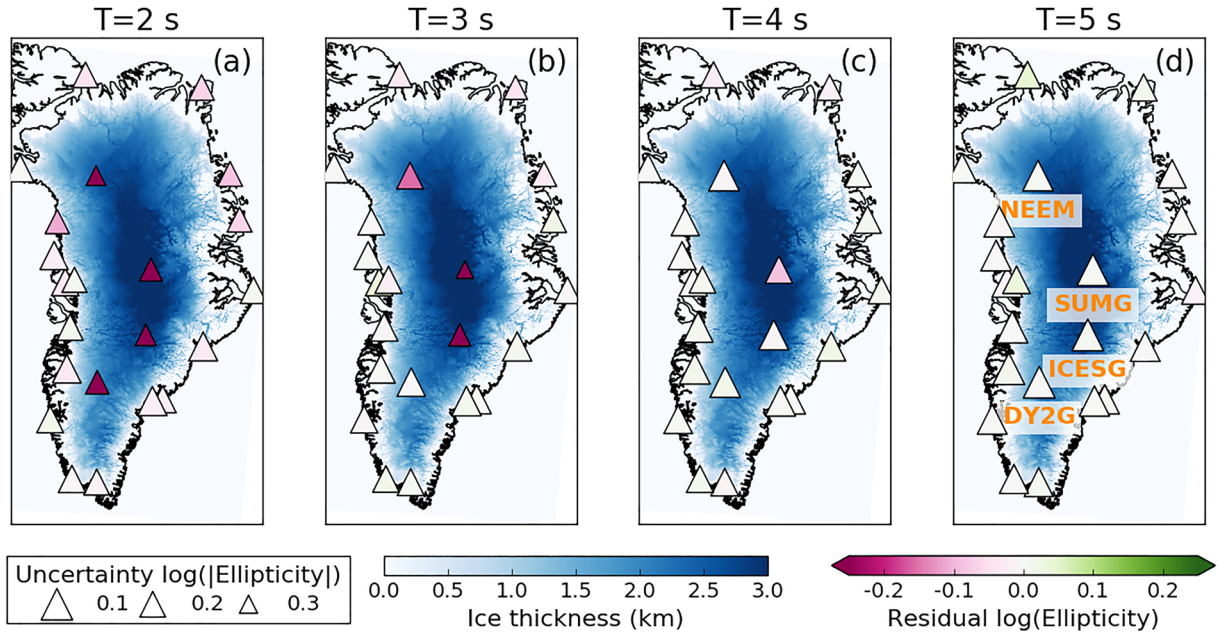

Figure 1. Map of ellipticity residuals between 2015 observations with a degree-of-polarisation (DOP) ≥0.95 (See Section 2.1 for more details about the DOP measurement method) and fundamental mode calculations from the model of Jones et al. (2021), as a function of period and ice thickness. The colors of the triangles are the ellipticity residuals with the size representing the uncertainty of each ellipticity measurement. The background color is the ice sheet thickness taken from the Bedmachine v3 model (Morlighem et al., 2017).

are a powerful tool for probing the subsurface in regions of sparse or limited station coverage and are seeing increasing applications in glaciological settings to determine ice thickness, seismic velocities and firn properties (Chaput et al., 2022; Köhler et al., 2019; Lévêque et al., 2010; Picotti et al., 2017; Preiswerk et al., 2019; Yan et al., 2018, 2020). Jones et al. (2021) extracted Rayleigh ellipticity measurements from ambient noise to determine a seismic velocity structure for the upper 5 km of the crust beneath Greenland. However, data with wave periods sensitive to the ice sheet ($T < 3$–4 s) show a strong deviation from theoretical fundamental mode Rayleigh wave ellipticity as well as larger measurement uncertainties relative to off-ice stations (Figures 1a and 1b and Figure S1 in Supporting Information S1).

Here we summarize the key features of Rayleigh wave ellipticity measurements made in 2015 from the four permanent on-ice stations in Greenland (DY2G, ICESG, SUMG, NEEM). To understand the source of the deviation between observed ellipticity measurements and predicted ellipticity for fundamental mode Rayleigh waves, we systematically test the effect of different 1-D ice sheet velocity and attenuation ($1/Q$) profiles on the ellipticity measurements, including potential overtone contamination effects. We generate several sets of synthetic seismic noise, which are processed in the same way as the real data and are compared with the observations of Jones et al. (2021).

2. Rayleigh Wave Ellipticity Results

2.1. DOP-E Method

Berbellini et al. (2019) developed the DOP-E method building upon the degree-of-polarisation (DOP) approach of Schimmel and Gallart (2003, 2004) and Schimmel et al. (2011) to identify and extract Rayleigh waves from ambient noise. DOP is an instantaneous quality measure based on the stability of polarisation properties of a signal within a window (e.g., Schimmel & Gallart, 2003, 2004; Schimmel et al., 2011; Sergeant et al., 2013). Polarisation properties are computed by a moving window eigen-decomposition of the time-frequency representation of three-component seismograms allowing for the calculation of the instantaneous semi-major and semi-minor axes of the best-fitting ellipse to the data (Schimmel & Gallart, 2003, 2004). Variability in polarisation properties is determined relative to the planarity vector, defined as the vector product of the semi-major and semi-minor axes which closely matches the expected particle motion of fundamental mode Rayleigh waves (e.g., Schimmel &

Gallart, 2003, 2004; Schimmel et al., 2011). DOP is computed as a projection of the instantaneous unit planarity vector on the mean planarity vector for the data window and ranges between 0 and 1, where 0 indicates randomly changing polarisation and 1 is a stable polarisation measurement throughout the data window (Berbellini et al., 2019; Jones et al., 2021; Schimmel & Gallart, 2003, 2004; Schimmel et al., 2011; Sergeant et al., 2013). For signals with DOP measurements above a given threshold, the period-dependent ellipticity of the data is computed (Berbellini et al., 2019; Jones et al., 2021).

2.2. Ellipticity Measurements

Ellipticity measurements made at stations in the GLISN network were obtained using the DOP-E method for wave periods of 2–10 s between 2012 and 2017 (Jones et al., 2021). A DOP of ≥0.95 was selected to ensure only the best measurements would be used when estimating the ellipticity. For each year, ellipticity curves are constructed from the distribution of measurements for each period by estimating the median and uncertainties at 13.6 and 84.6 percentiles (Berbellini et al., 2019; Jones et al., 2021). We observe some seasonal variation in ellipticity with early summer months (May–July) having lower relative values of ellipticity and early winter (November–January) values above the annual average (Figures S2–S5 in Supporting Information S1). Annual ellipticity estimates do not vary significantly between years, and for the present study, we analyze the 2015 ellipticity measurements presented by Jones et al. (2021).

The ellipticity measurements are highly sensitive to the ice thickness showing a characteristic inflection at $T \sim 3$–4 s (Figure S1 in Supporting Information S1), which is not observed on off-ice stations (Figure S1 in Supporting Information S1; Jones et al., 2021). For on-ice stations at periods sensitive to the ice ($T < 3$–4 s) a strong deviation from fundamental mode ellipticity predictions occurs, with the thickest ice stations, SUMG and ICESG, showing the greatest difference (Figure 1 and Figure S1 in Supporting Information S1). We also observe that the uncertainties in ellipticity measurements are larger at on-ice stations at periods sensitive to the ice (Figure 1 and Figure S1 in Supporting Information S1).

The predominant source of the Rayleigh waves is in the North Atlantic between Greenland and Iceland, with dominant periods between 5 and 10 s (Sergeant et al., 2013; Jones et al., 2021, Figures S6–S9 in Supporting Information S1). We observe a 180° rotation in the source of the Rayleigh waves at ∼2.2 s (0.45 Hz) and ∼3 s (0.3 Hz) for stations ICESG and SUMG respectively (Figures S7 and S8 in Supporting Information S1). Inherent to the DOP-E method is the assumption that the particle motion of the Rayleigh wave has a retrograde motion (Schimmel et al., 2011; Sergeant et al., 2013). A 180° rotation in the source-receiver back azimuth at high frequencies suggests a change in the Rayleigh wave particle motion from retrograde to prograde motion. Changes in the fundamental mode Rayleigh wave particle motion have been observed in settings with large subsurface seismic velocity contrasts, such as firn layers in West Antarctica (Chaput et al., 2022) and sedimentary basins (e.g., Berbellini et al., 2016; Tanimoto & Rivera, 2005). Moreover, these settings with large velocity contrasts often give rise to Rayleigh wave overtones (e.g., Ma et al., 2016), which are also associated with prograde ellipticity measurements (Figures S7 and S8 in Supporting Information S1).

3. Numerical Simulations

3.1. Synthetic Noise Generation

To understand the main causes of our anomalous observations of short-period Rayleigh wave ellipticity, we measure ellipticity from 24 hr of simulated ambient noise data following the approach of Berbellini et al. (2019). The synthetic seismograms are computed up to the fifth overtone and down to a wave period of $T = 1$ s for different 1-D ice sheet velocity models and seismic Q profiles at stations DY2G, ICESG, SUMG and NEEM (Figure 1). Synthetic seismograms are computed using normal mode summation (Gilbert, 1971) using the software package of Herrmann (2013), where normal mode eigenfunctions and eigenvalues are computed and combined with an appropriate source term. We simulate microseismic Rayleigh waves as 300 vertical orientated impulsive point sources evenly spaced over 24 hr with random amplitudes selected from a uniform distribution between 10^{12} and 10^{16} N m (Berbellini et al., 2019). In order to make our synthetic noise more realistic, we combine these vertical point sources with 200 horizontally orientated double couple sources with amplitudes from a uniform distribution between 10^{12} and 10^{16} N m (Berbellini et al., 2019). Sources are located in the Irminger Sea, North Atlantic, which is a region of strong microseismic sources (Sergeant et al., 2013) and are selected from a random

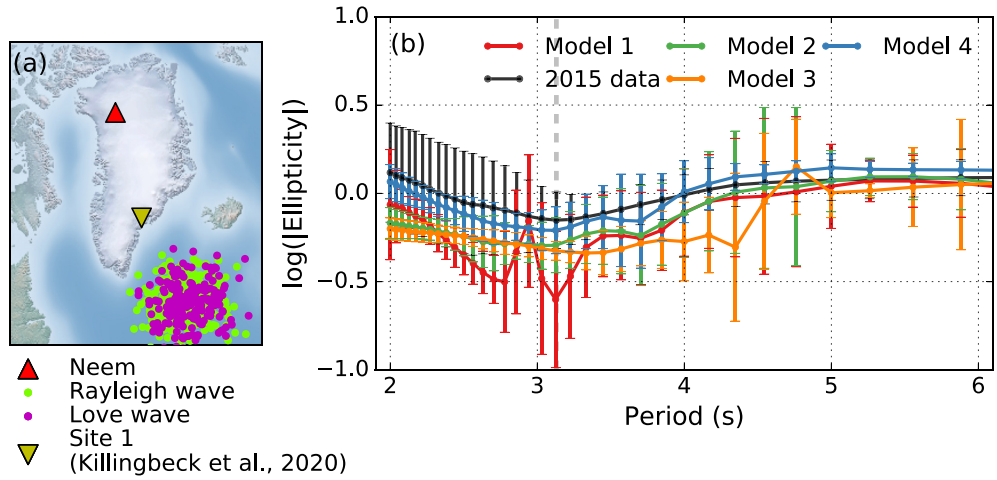

Figure 2. (a) Map showing the location of the vertical and double couple sources for the generation of the synthetic seismic noise. The green circles are the vertical Rayleigh wave sources and the pink circles are the horizontal double couple sources for the Love waves, the seismic station NEEM is a red triangle and the yellow triangle is the location of Site 1 from Killingbeck et al. (2020). (b) Plot comparing the 2015 ellipticity measurements from NEEM station and measurements made from synthetic data generated using different velocity models. Model 1 is a single homogeneous ice layer, Model 2 consists of a homogeneous ice layer overlain by firn based on the results of Killingbeck et al. (2020), Model 3 comprises a homogeneous ice layer underlain by a thin dilatant sediment/till and Model 4 consists of a homogeneous ice layer with a near surface layer derived from an exploratory parameter search (see Section 3.1 for further details).

2-D Gaussian distribution centered on 57°N and 31°W, with a standard deviation of ±2°N and ±4°W (Figure 2; Berbellini et al., 2019). The sources are located at a depth of 2.3 km corresponding to the average seafloor depth of the source region. Finally, we add Gaussian noise with a standard deviation which leads to ambient noise synthetics with a root-mean-squared (RMS) signal-to-noise ratio of ten.

3.2. Velocity Models

We test four velocity models representing different expected ice and subglacial environments. Model 1 is a single homogeneous ice layer with Vp = 3.80 km/s, Vs = 1.94 km/s and ρ = 915 kg/m^3 (Jones et al., 2021); Model 2 contains a firn layer with parameters based on the geophysical observations of Killingbeck et al. (2020) in East Greenland. The model consists of 3 layers with thicknesses of 20 m, 10 m, 20 m, Vp = (2.20, 3.10, 3.40) km/s, Vs = (1.00, 0.99, 1.50) km/s and ρ = (716, 882, 883) kg/m^3, respectively, which were calculated as the average properties at Site 1 at an elevation of 1,770 m (Figure 2; Killingbeck et al., 2020). Model 3 comprises a homogeneous ice layer underlain by a thin dilatant sedimentary/till layer 10 m thick with Vp = 1.80 km/s, Vs = 0.20 km/s and ρ = 1,900 kg/m^3 (Booth et al., 2012). The final model, "Model 4", was selected using the Neighborhood Algorithm (Sambridge, 1999) to search for candidate models for a single near surface layer with a variable thickness up to 50 m and velocities and density in the following ranges; Vp = [0.20, 4.00] km/s Vs = [0.00, 2.00] km/s, ρ = [200, 1,100] kg/m^3 by matching the modeled fundamental mode Rayleigh wave ellipticity and measured data. Due to the large parameter space compared to the number of data points our attempt to invert for this near surface layer resulted in solutions which failed to fully converge or solutions with non-physical Vp/Vs ratios and as such the model with the lowest misfit is set as the preferred "Model 4" for each station (Table S1 in Supporting Information S1). During the model search the contributions of Rayleigh waves overtones were not considered. In all "Model 4" models Vs is extremely low, varying between 0.02 and 0.04 km/s. For all models, the ice thickness matches the Bedmachine v3 model (Morlighem et al., 2017).

We apply the DOP-E method to the synthetic seismograms computed for each velocity model exactly in the same way as with real data, using a sliding window. For each window, we compute the ellipticity keeping only those values with a DOP ≥0.95. For each model, ellipticity curves are then estimated from the distribution of measurements made on the synthetic noise data. Figure 2 compares the ellipticity measurements made on the synthetic seismograms with the observations from 2015 at NEEM station. In all examples, the ellipticity measurements with wave periods insensitive to the ice sheet (T > 4.5 s) match the geological model as expected (Figures 2 and

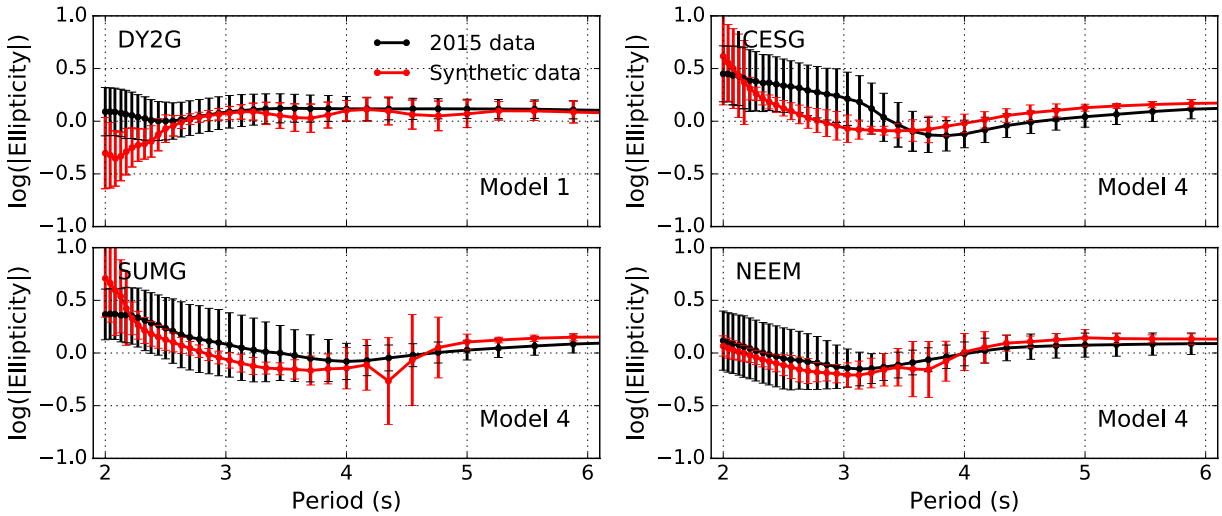

Figure 3. Summary plot of ellipticity as a function of period, comparing the 2015 measurements with measurements made on synthetic data from the best fitting model at stations DY2G, ICESG, SUMG, and NEEM. For DY2G the single ice layer model was selected whilst for ICESG, SUMG and NEEM the firn layer inferred from an exploratory inversion was deemed to best represent the trends of the data.

Figures S10–S13 in Supporting Information S1). In Model 1 at $T \sim 3$–4 s the synthetic ellipticity curve comprises a combination of the fundamental mode, first and second overtones which is followed by a sharp peak in ellipticity at $T = 2.9$ s where the second overtone becomes dominant (Figure S14 in Supporting Information S1). At $T < 2.9$ s the ellipticity measurements are dominated by the first overtone (Figure S14 in Supporting Information S1). This change in dominance between the fundamental mode and overtones is seen in the other stations using Model 1 with varying degrees of prominence (Figure S14 in Supporting Information S1). Histograms of the ellipticity measurements typically depict a distribution consisting of a single large peak (Figures S15–S18 in Supporting Information S1). However, some models for example, Model 1 at $T = 2$ s at NEEM and SUMG stations (Figures S17 and S18 in Supporting Information S1) depict a bimodal distribution with each of the peaks corresponding to either the fundamental mode or the first or second overtones. Figure 2 and S10–S13 show that the ellipticity predictions from Model 1 do not match the ice-sensitive observations ($T < 3$–4 s). Hence, a simple ice layer does not explain the measured ellipticity, even when considering the potential presence of overtones.

The inclusion of a firn layer (Model 2) does not explain the measured ellipticity either (Figure 2 and Figures S10–S13 in Supporting Information S1). The addition of a soft saturated sediment or till layer at the base of the ice in Model 3 results in an increase in the wave period marking the transition between the bedrock and ice layer. For example, at NEEM the transition between ice-to-rock sensitive periods occurs at $T \sim 3.5$ s for the real data as well as Models 1, 2, and 4, whilst the addition of sediment at the ice bedrock interface in Model 3 pushed the transition to $T \sim 4.5$ s (Figure 2).

Measurements from synthetics computed for each Model 4 for each station reproduce well the general trend of rapidly increasing ellipticity for periods sensitive to the ice at all stations except for DY2G (Figures S10–S13 in Supporting Information S1). A good match between the synthetics generated using Model 4 for NEEM station and field measurements is seen in Figure 2. At SUMG there is a secondary linear trend observed for $T < 2.5$ s which is caused by the excitation of the first overtone (Figure 3, Figure S19 in Supporting Information S1). Figure 3 compares synthetic measurements for the velocity models which best capture the overall trend of the 2015 observations. At ICESG, SUMG and NEEM Model 4 matches the overall trend in ellipticity whilst at DY2G there is little variation between the different candidate models, with none of them explaining the short period ($T < 2.8$ s) trend in ellipticity.

3.3. Variations in Q

Variations in the velocity structure of the ice column are to first order compatible with our anomalous ellipticity measurements at wave periods sensitive to the ice (Figures 2 and 3). However, the distributions of the ellipticity observations are much broader for ice sensitive wave periods than their counterparts measured from the synthetic

data (Figures S12–S15). Seismic attenuation arises due to a loss of seismic energy during propagation due to anelastic effects for example, internal friction and scattering and is sensitive to the thermal state, ice density, crystallographic orientation of ice and the frequency of the seismic waves (e.g., Peters et al., 2012; Podolskiy & Walter, 2016). The seismic quality factor Q (i.e., the inverse of attenuation) can vary significantly in ice from 5 to 1,000 depending on length scale (e.g., Toyokuni et al., 2021) and temperature (Kuroiwa, 1964; Peters et al., 2012). For example, Kuroiwa (1964) conducted laboratory experiments on ice samples from Greenland and the Antarctic observing Qp $\sim$ 40 at 0°C and Qp $\sim$ 1,000 at −30°C. Qs has been shown to have a significant effect on Rayleigh waves composition at short periods where higher order overtones can experience up to two to three times less attenuation than the fundamental mode, which suggests that ellipticity measurements may include different numbers of Rayleigh wave overtones (Dahlen & Tromp, 1999; Hariharan et al., 2022).

We investigate the effect of attenuation on ellipticity measurements made on synthetic seismograms using the single ice column velocity model (Model 1). We opt to use a single ice layer model due to its simplicity allowing for better isolation of the effects of Q on the observations. We use Qp = Qs = [20, 50, 175, ∞] for the values of Q for the ice layer based on the study of Toyokuni et al. (2021), with the sub-ice seismic structure assigned values derived from PREM (Dziewonski & Anderson, 1981). Figure 4 compares the distribution of the ellipticity measurements made on the synthetic seismograms with a Gaussian distribution estimated using 2015 ellipticity data curves for the station NEEM. At periods $T \leq 4$ s the measurements made on the synthetic seismograms do not produce a Gaussian distribution. We observe that the values of Qp = Qs = [175, ∞] produce similar histogram distributions dominated by a single peak (Figure 4 and Figures S23–S26 in Supporting Information S1). However, for values of Qp = Qs = [20,50] at $T = 4$ s the distribution of synthetic measurements changes into a bimodal distribution ($T = 3$ s, Figure 4). Similar reshaping of the synthetic ellipticity distributions has a dramatic effect on the ellipticity curves as seen in Figures S20–S23 in Supporting Information S1. We also note that at $T = 5$ s Qp = Qs = 20 produces the best distribution of measurements which matches the Gaussian probability density function from the 2015 ellipticity data.

4. Discussion

We have systematically tested the different effects of the seismic velocity and attenuation of the ice column on Rayleigh wave ellipticity, by computing synthetic ellipticity measurements for on-ice stations in Greenland and comparing them with real observations (Jones et al., 2021). We found that using a single ice layer did not explain the real ellipticity observations (Figure 2). The addition of sediment/till at the ice sheet base produced a shallowing and movement of the inflection in ellipticity to longer periods, which is not compatible with the observations. Moreover, we found that the geophysically constrained firn layer (Killingbeck et al., 2020) is also unable to match the observed ellipticity (Figure 2). The inclusion of a thin layer just below the surface ~10 m thick with Vp = 1–2 km/s, $\rho \sim 800$ kg/m^3 and Vs $\sim$ 0.02 km/s, allowed us to fit the general ellipticity trend seen in the measured data for ice sensitive periods (Figure 3). These values of Vp and ρ are consistent with expected values for firn (e.g., Albert, 1998; Chaput et al., 2022; Killingbeck et al., 2020) whilst the low Vs values are consistent with values estimated for dry snow (e.g., Guillemot et al., 2021). At station NEEM we observe a very good match between the synthetic and observed ellipticity with no contribution from overtones (Figures 2 and 3). At stations ICESG and SUMG we observe contributions from the first overtones at periods of $T \sim 2$ s (Figure 3). SUMG, ICESG, and NEEM are characterized by dry snow conditions and experience little summer melt (e.g., Vandecrux et al., 2020) and, as such, we interpret the shallow near surface layer, which captures the main features of the ellipticity curves, as snow transitioning to firn.

Firn and snow layers introduce steep seismic vertical velocity gradients which lead to complex seismic wave propagation, including site amplification effects, wind snow excited resonances as well as 2D and 3D effects (e.g., Chaput et al., 2018; Chaput et al., 2022) which are not accounted for in our modeling. These could account for the differences between the synthetic and real ellipticity measurements seen at stations ICESG and SUMG (Chaput et al., 2018, 2022). Also, ellipticity measurements from the synthetic data associated with overtones did not produce ellipticity curves consistent with the real observations and as such these overtones are not responsible for the prograde Rayleigh wave particle motion at ICESG and SUMG. The sharp velocity contrast of the near surface layer can give rise to prograde fundamental model Rayleigh wave particle motions (Figure S27 in Supporting Information S1), similar to observations made in firn layers in West Antarctica (Chaput et al., 2022), or sedimentary basins (Berbellini et al., 2016; Tanimoto & Rivera, 2005). We also acknowledge other potential mechanisms, such resonance of the ice sheet and firn, that may also be responsible for the prograde motion.

The models obtained from Test 4 led to synthetic ellipticity curves that matched well the general trends of the real observed ellipticity at stations ICESG, SUMG and NEEM, but none can explain the short period variations

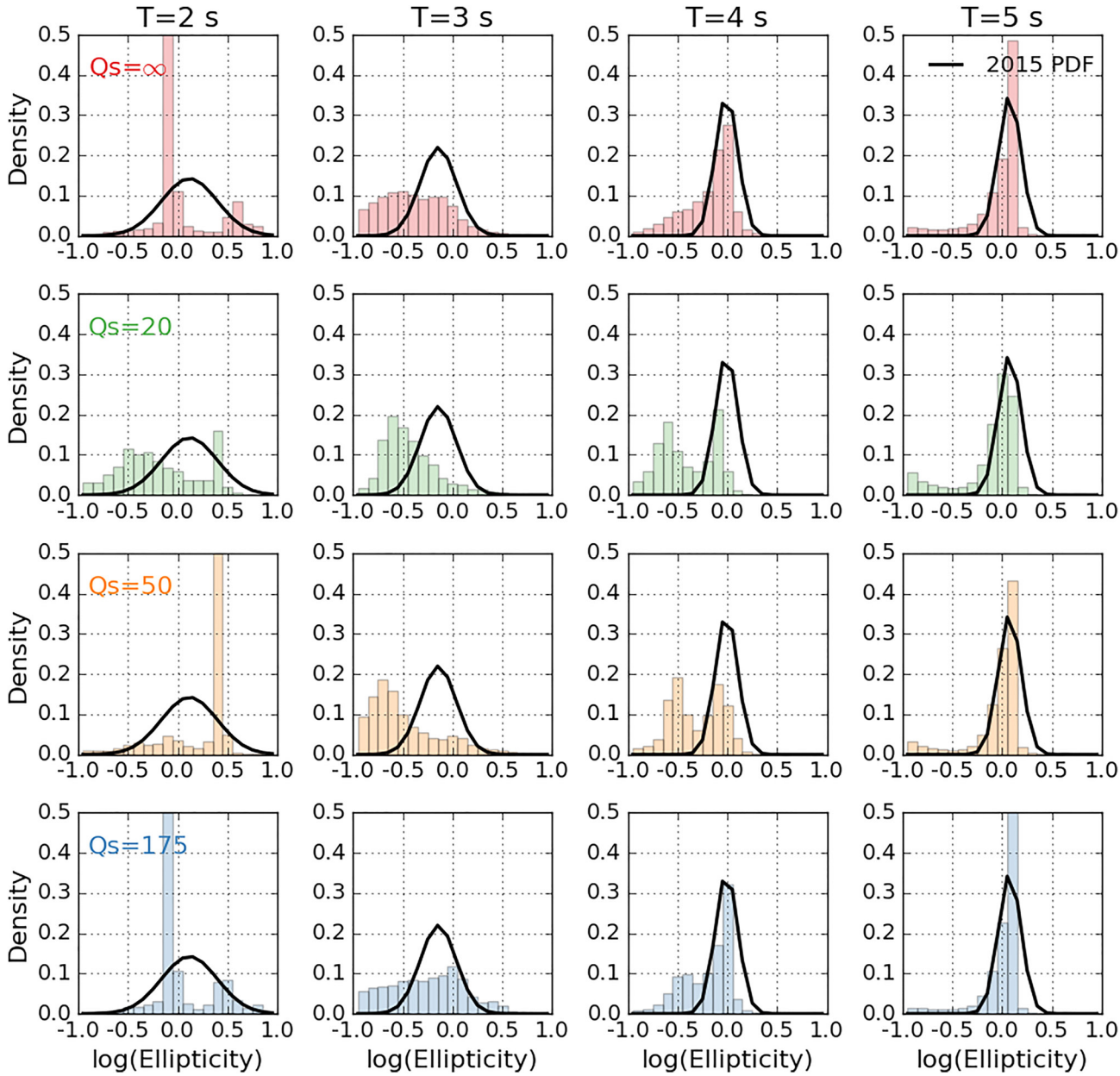

Figure 4. Histograms of the distribution of ellipticity measurements as a function of the period ($T = 2, 3, 4, 5$s) for different values of Q for station NEEM. The solid black line is the Gaussian probability density function estimated from the 2015 ellipticity curves.

in ellipticity at station DY2G (Figure 3). DY2G is located in the ablation zone where the snow is typically wet and the region experiences annual melting and re-freezing cycles (e.g., Vandecrux et al., 2020). This thaw and re-freezing cycle along with snow accumulation can have a significant effect on the near-surface temperature, density and seismic velocities (Vandecrux et al., 2020). Annual ellipticity curves in the ablation zone cannot capture the temporal variations in seismic properties in such a dynamic environment (Figure S1 in Supporting Information S1). A limitation of this study is the assumption that the Rayleigh wave ellipticity is sensitive to the 1-D subsurface structure which may not be fully valid at shorter periods ($T < 3$ s), especially in regions with significant subglacial topography. In such regions, 3D effects for example, subglacial geometry can lead to Rayleigh wave resonance which could greatly affect the ellipticity observations (Preiswerk et al., 2019). Nevertheless, ellipticity could be an ideally suited technique for the temporal monitoring of both ice thickness and surface meltwater.

Despite the success of varying the near surface velocity structure of the ice in describing the observed short periods in ellipticity, the distributions of the observations from 2015 are much broader for ice sensitive periods than

their counterparts measured from the synthetic data. The broadening of the distribution of the ellipticity measurements is confined only to on-ice stations (Jones et al., 2021). Q has been shown to be highly sensitive to the thermal state of ice (e.g., Kuroiwa, 1964; Peters et al., 2012). Therefore the accurate estimation of Q can be used as a tool for monitoring cryohydrological warming. Moreover, as mentioned previously surface wave sensitivity to Qs has been shown to depend on the overtone number where at short periods higher order overtones can experience two to three times less attenuation than the fundamental mode (Dahlen & Tromp, 1999; Hariharan et al., 2022). Accurate estimates of Q for the ice will also provide additional constraints in the modeling of Rayleigh wave ellipticity and inversion for ice structure.

Using a single ice column model we showed that seismic attenuation values of Qp and Qs of ∼50 lead to a broadening of the distribution of the ellipticity measurements uncertainties comparable with the 2015 observations at periods sensitive to the ice (Figure 4). These results are consistent with the study of Toyokuni et al. (2021), which found that the GrIS has low values of Q (Qp and Qs $\leq$ 50). We also note that Qp = Qs = 175 produces results similar to the models with no attenuation (i.e., $Q = \infty$) implying that a Qp and Qs of 175 is an upper estimate for the GrIS. Due to the frequency dependence of Q, a direct comparison with the results of Peters et al. (2012) is not possible, however, based on their analysis values of $Q < 100$ typically corresponded with relatively warm ice temperatures of $>-10°$. These temperatures are corroborated by Kuroiwa (1964) where Qp ∼ 40 was observed around 0°C. Our results show the incorporation of Q into an inversion scheme can be used as a tool to monitor seasonal and annual changes in the thermal component of the ice sheet and its response to cryohydrological warming and will be the subject of further work.

The permanent deployment of the GLISN network provides an opportunity to use Rayleigh wave ellipticity to quantify and study changes in ice temperature and the evolution of the firn on the GrIS on a monthly, seasonal and annual basis. An inversion strategy to determine the ice structure should consider ellipticity measurements made on synthetic noise as the forward modeling operator with the objective function comparing not only the ellipticity curves as done previously (e.g., Attanayake et al., 2017; Berbellini et al., 2017; Ferreira et al., 2020; Jones et al., 2021; Yano et al., 2009) but also including the distribution of each measurement as well as any indicators of changes in Rayleigh wave polarisation for example, 180° reversal in source azimuth (Figures S2–S5 in Supporting Information S1). Finally, the addition of Rayleigh wave dispersion measurements may also help constrain the thermal and mechanical structure of the ice and any seasonal variations.

5. Conclusions

We have shown that the GrIS has a profound effect on Rayleigh wave ellipticity, leading to substantial differences between observations and fundamental mode Rayleigh wave predictions for wave periods sensitive to ice (typically $T < 3$–4 s for the existing permanent on-ice stations in Greenland). To understand these unexpected variations and complexity in ellipticity observations we simulated 24 hr of seismic ambient noise for different 1-D ice sheet profiles and measured the corresponding ellipticity. Our findings show that in dry snow conditions within the interior of the GrIS, ellipticity is sensitive to the accumulation and densification of snow into firn, resulting in complex seismic wave propagation and subsequent ellipticity. However, within the wet snow conditions of the ablation zone, average annual estimates of ellipticity are not appropriate for capturing the thaw-freeze cycles. We show that variations in ellipticity are affected by seismic attenuation which is sensitive to the thermal structure of the ice. Our study shows that Rayleigh wave ellipticity is an ideal method for the monitoring of firn compaction, massive ice formation, firn aquifer development or expansion, or temperature changes of the main bodies of ice sheets, shelves or glaciers. This matters not only in Greenland where future climate warming is predicted to transform the ice sheet's snow, firn and ice columns at progressively higher altitudes and latitudes but also in respect of the predicted Greenlandification of a warming Antarctic Ice Sheet in the coming decades to centuries.

Data Availability Statement

The seismic data were acquired and distributed by the Greenland Ice Sheet Monitoring Network (GLISN) federation and its members (http://ds.iris.edu/mda/_GLISN/?timewindow=2013/01/10%2010:00:30-2599/12/31%2023:59:59). The virtual network code for GLISN is _GLISN with the network codes DK used for DY2G, ICESG and NEEM and GE at SUMG. The facilities of IRIS Data Services, and specifically the IRIS Data Management Center, were used for access to waveforms, related metadata, and/or derived products used in this study (https://ds.iris.edu/ds/nodes/dmc/). The figures were created using the Matplotlib package (Hunter, 2007). The python toolbox obspyDMT (Hosseini & Sigloch, 2017) was used to download the seismic data. The DOP-E processing code was downloaded and distributed from: github.com/berbellini/DOP-E.

Acknowledgments
G.A.J. is funded by the Sêr Cymru II Program in Low Carbon Energy and the Environment (European Regional Development Fund and Welsh European Funding Office; Project number 80761-SU-SU093). A.M.G.F. is grateful to support from NERC Grant NE/N011791/1. M.S. thanks SANIMS (RTI2018-095594-B-I00). This project has received funding from the European Research Council (ERC) under the European Union's Horizon 2020 research and innovation program (grant agreement No 101001601). IRIS Data Services are funded through the Seismological Facilities for the Advancement of Geoscience (SAGE) Award of the National Science Foundation under Cooperative Support Agreement EAR-1851048.

References

Abram, N., Carolina, A., Bindoff, N., & Cheng, L. (2019). Special report on the ocean and cryosphere in a changing climate. *Intergovernmental Panel on Climate Change*, *1*, 1–36.

Albert, D. G. (1998). Theoretical modeling of seismic noise propagation in firn at the south pole, Antarctica. *Geophysical Research Letters*, *25*(23), 4257–4260. https://doi.org/10.1029/1998gl900155

Anandakrishnan, S., Blankenship, D., Alley, R., & Stoffa, P. (1998). Influence of subglacial geology on the position of a West Antarctic ice stream from seismic observations. *Nature*, *394*(6688), 62–65. https://doi.org/10.1038/27889

Attanayake, J., Ferreira, A. M., Berbellini, A., & Morelli, A. (2017). Crustal structure beneath Portugal from teleseismic Rayleigh wave ellipticity. *Tectonophysics*, *712*, 344–361. https://doi.org/10.1016/j.tecto.2017.06.001

Berbellini, A., Morelli, A., & Ferreira, A. M. (2016). Ellipticity of Rayleigh waves in basin and hard-rock sites in northern Italy. *Geophysical Journal International*, *206*(1), 395–407. https://doi.org/10.1093/gji/ggw159

Berbellini, A., Morelli, A., & Ferreira, A. M. (2017). Crustal structure of northern Italy from the ellipticity of Rayleigh waves. *Physics of the Earth and Planetary Interiors*, *265*, 1–14. https://doi.org/10.1016/j.pepi.2016.12.005

Berbellini, A., Schimmel, M., Ferreira, A. M., & Morelli, A. (2019). Constraining S-wave velocity using Rayleigh wave ellipticity from polarization analysis of seismic noise. *Geophysical Journal International*, *216*(3), 1817–1830. https://doi.org/10.1093/gji/ggy512

Booth, A., Clark, R., Kulessa, B., Murray, T., Carter, J., Doyle, S., & Hubbard, A. (2012). Thin-layer effects in glaciological seismic amplitude-versus-angle (ava) analysis: Implications for characterising a subglacial till unit, Russell glacier, west Greenland. *The Cryosphere*, *6*(4), 909–922. https://doi.org/10.5194/tc-6-909-2012

Change, I. P. O. C. (2014). *Climate change 2013: The physical science basis: Working group i contribution to the fifth assessment report of the intergovernmental panel on climate change*. Cambridge University Press.

Chaput, J., Aster, R., Karplus, M., & Nakata, N. (2022). Ambient high-frequency seismic surface waves in the firn column of central west Antarctica. *Journal of Glaciology*, *68*(270), 1–14. https://doi.org/10.1017/jog.2021.135

Chaput, J., Aster, R., McGrath, D., Baker, M., Anthony, R. E., Gerstoft, P., et al. (2018). Near-surface environmentally forced changes in the Ross Ice Shelf observed with ambient seismic noise. *Geophysical Research Letters*, *45*(20), 11–187. https://doi.org/10.1029/2018gl079665

Cuffey, K. M., & Paterson, W. S. B. (2010). *The physics of glaciers*. Academic Press.

Dahlen, F., & Tromp, J. (1999). *Theoretical global seismology*. Princeton university press.

Davison, B. J., Sole, A. J., Livingstone, S. J., Cowton, T. R., & Nienow, P. W. (2019). The influence of hydrology on the dynamics of land-terminating sectors of the Greenland ice sheet. *Frontiers in Earth Science*, *10*. https://doi.org/10.3389/feart.2019.00010

Dziewonski, A. M., & Anderson, D. L. (1981). Preliminary reference earth model. *Physics of the Earth and Planetary Interiors*, *25*(4), 297–356. https://doi.org/10.1016/0031-9201(81)90046-7

Ferreira, A. M., Marignier, A., Attanayake, J., Frietsch, M., & Berbellini, A. (2020). Crustal structure of the Azores Archipelago from Rayleigh wave ellipticity data. *Geophysical Journal International*, *221*(2), 1232–1247. https://doi.org/10.1093/gji/ggaa076

Ferreira, A. M., & Woodhouse, J. H. (2007). Source, path and receiver effects on seismic surface waves. *Geophysical Journal International*, *168*(1), 109–132. https://doi.org/10.1111/j.1365-246x.2006.03092.x

Gilbert, F. (1971). Excitation of the normal modes of the earth by earthquake sources. *Geophysical Journal International*, *22*(2), 223–226. https://doi.org/10.1111/j.1365-246x.1971.tb03593.x

Guillemot, A., van Herwijnen, A., Larose, E., Mayer, S., & Baillet, L. (2021). Effect of snowfall on changes in relative seismic velocity measured by ambient noise correlation. *The Cryosphere*, *15*(12), 5805–5817. https://doi.org/10.5194/tc-15-5805-2021

Hariharan, A., Dalton, C. A., Babikoff, J., & Ekström, G. (2022). Controls on surface wave overtone interference. *Geophysical Journal International*, *228*(3), 1665–1683. https://doi.org/10.1093/gji/ggab424

Herrmann, R. B. (2013). Computer programs in seismology: An evolving tool for instruction and research. *Seismological Research Letters*, *84*(6), 1081–1088. https://doi.org/10.1785/0220110096

Hosseini, K., & Sigloch, K. (2017). ObspyDMT: A Python toolbox for retrieving and processing large seismological data sets. *Solid Earth*, *8*(5), 1047–1070. https://doi.org/10.5194/se-8-1047-2017

Hunter, J. D. (2007). Matplotlib: A 2d graphics environment. *Computing in Science & Engineering*, *9*(3), 90–95. https://doi.org/10.1109/MCSE.2007.55

Jones, G. A., Ferreira, A. M., Kulessa, B., Schimmel, M., Berbellini, A., & Morelli, A. (2021). Uppermost crustal structure regulates the flow of the Greenland ice sheet. *Nature Communications*, *12*(1), 1–12. https://doi.org/10.1038/s41467-021-27537-5

Killingbeck, S., Schmerr, N., Montgomery, L., Booth, A., Livermore, P., Guandique, J., et al. (2020). Integrated borehole, radar, and seismic velocity analysis reveals dynamic spatial variations within a firn aquifer in southeast Greenland. *Geophysical Research Letters*, *47*(18), e2020GL089335. https://doi.org/10.1029/2020gl089335

Köhler, A., Maupin, V., Nuth, C., & Van Pelt, W. (2019). Characterization of seasonal glacial seismicity from a single-station on-ice record at Holtedahlfonna, Svalbard. *Annals of Glaciology*, *60*(79), 23–36. https://doi.org/10.1017/aog.2019.15

Kuroiwa, D. (1964). Internal friction of ice. III; the internal friction of natural glacier ice. *Contributions from the Institute of Low Temperature Science*, *18*, 49–62.

Lévêque, J.-J., Maggi, A., & Souriau, A. (2010). Seismological constraints on ice properties at dome c, Antarctica, from horizontal to vertical spectral ratios. *Antarctic Science*, *22*(5), 572–579. https://doi.org/10.1017/s0954102010000325

Ma, Y., Clayton, R. W., & Li, D. (2016). Higher-mode ambient-noise Rayleigh waves in sedimentary basins. *Geophysical Journal International*, *206*(3), 1634–1644. https://doi.org/10.1093/gji/ggw235

Mordret, A., Mikesell, T. D., Harig, C., Lipovsky, B. P., & Prieto, G. A. (2016). Monitoring southwest Greenland's ice sheet melt with ambient seismic noise. *Science Advances*, *2*(5), e1501538. https://doi.org/10.1126/sciadv.1501538

Morlighem, M., Williams, C. N., Rignot, E., An, L., Arndt, J. E., Bamber, J. L., et al. (2017). BedMachine v3: Complete bed topography and ocean bathymetry mapping of Greenland from multibeam echo sounding combined with mass conservation. *Geophysical Research Letters*, *44*(21), 11–051. https://doi.org/10.1002/2017gl074954

Peters, L., Anandakrishnan, S., Alley, R., & Voigt, D. (2012). Seismic attenuation in glacial ice: A proxy for englacial temperature. *Journal of Geophysical Research*, *117*(F2), F02008. https://doi.org/10.1029/2011jf002201

Phillips, T., Rajaram, H., & Steffen, K. (2010). Cryo-hydrologic warming: A potential mechanism for rapid thermal response of ice sheets. *Geophysical Research Letters*, *37*(20), L20503. https://doi.org/10.1029/2010gl044397

Picotti, S., Francese, R., Giorgi, M., Pettenati, F., & Carcione, J. M. (2017). Estimation of glacier thicknesses and basal properties using the horizontal-to-vertical component spectral ratio (HVSR) technique from passive seismic data. *Journal of Glaciology*, *63*(238), 229–248. https://doi.org/10.1017/jog.2016.135

Podolskiy, E. A., & Walter, F. (2016). Cryoseismology. *Reviews of Geophysics*, *54*(4), 708–758. https://doi.org/10.1002/2016rg000526

Preiswerk, L. E., Michel, C., Walter, F., & Fäh, D. (2019). Effects of geometry on the seismic wavefield of alpine glaciers. *Annals of Glaciology*, *60*(79), 112–124. https://doi.org/10.1017/aog.2018.27

Sambridge, M. (1999). Geophysical inversion with a neighbourhood algorithm—I. Searching a parameter space. *Geophysical Journal International*, *138*(2), 479–494. https://doi.org/10.1046/j.1365-246x.1999.00876.x

Schimmel, M., & Gallart, J. (2003). The use of instantaneous polarization attributes for seismic signal detection and image enhancement. *Geophysical Journal International*, *155*(2), 653–668. https://doi.org/10.1046/j.1365-246x.2003.02077.x

Schimmel, M., & Gallart, J. (2004). Degree of polarization filter for frequency-dependent signal enhancement through noise suppression. *Bulletin of the Seismological Society of America*, *94*(3), 1016–1035. https://doi.org/10.1785/0120030178

Schimmel, M., Stutzmann, E., Ardhuin, F., & Gallart, J. (2011). Polarized Earth's ambient microseismic noise. *Geochemistry, Geophysics, Geosystems*, *12*(7), Q07014. https://doi.org/10.1029/2011gc003661

Sergeant, A., Stutzmann, E., Maggi, A., Schimmel, M., Ardhuin, F., & Obrebski, M. (2013). Frequency-dependent noise sources in the North Atlantic Ocean. *Geochemistry, Geophysics, Geosystems*, *14*(12), 5341–5353. https://doi.org/10.1002/2013gc004905

Tanimoto, T., & Rivera, L. (2005). Prograde Rayleigh wave particle motion. *Geophysical Journal International*, *162*(2), 399–405. https://doi.org/10.1111/j.1365-246x.2005.02481.x

Toyokuni, G., Komatsu, M., & Takenaka, H. (2021). Estimation of seismic attenuation of the Greenland ice sheet using 3-D waveform modeling. *Journal of Geophysical Research: Solid Earth*, *126*(4), e2021JB021694. https://doi.org/10.1029/2021jb021694

Toyokuni, G., Takenaka, H., Takagi, R., Kanao, M., Tsuboi, S., Tono, Y., et al. (2018). Changes in Greenland ice bed conditions inferred from seismology. *Physics of the Earth and Planetary Interiors*, *277*, 81–98. https://doi.org/10.1016/j.pepi.2017.10.010

Vandecrux, B., Mottram, R., Langen, P. L., Fausto, R. S., Olesen, M., Stevens, C. M., et al. (2020). The firn meltwater retention model intercomparison project (RETMIP): Evaluation of nine firn models at four weather station sites on the Greenland ice sheet. *The Cryosphere*, *14*(11), 3785–3810. https://doi.org/10.5194/tc-14-3785-2020

Yan, P., Li, Z., Li, F., Yang, Y., & Hao, W. (2020). Antarctic ice-sheet structures retrieved from p-wave coda autocorrelation method and comparisons with two other single-station passive seismic methods. *Journal of Glaciology*, *66*(255), 153–165. https://doi.org/10.1017/jog.2019.95

Yan, P., Li, Z., Li, F., Yang, Y., Hao, W., & Bao, F. (2018). Antarctic ice sheet thickness estimation using the horizontal-to-vertical spectral ratio method with single-station seismic ambient noise. *The Cryosphere*, *12*(2), 795–810. https://doi.org/10.5194/tc-12-795-2018

Yano, T., Tanimoto, T., & Rivera, L. (2009). The ZH ratio method for long-period seismic data: Inversion for S-wave velocity structure. *Geophysical Journal International*, *179*(1), 413–424. https://doi.org/10.1111/j.1365-246x.2009.04293.x